Excitation Dispersion from Inelastic Low-Energy Electron Diffraction

J. O. Porteus and W. N. Faith
Michelson Laboratory, China Lake, California 93555
(Received 24 November 1969; revised manuscript received 24 April 1970)

Combined inelastic scattering and diffraction (inelastic diffraction) provide a means of observing low-energy electrons which have produced electronic excitation in bulk single crystals. In principle, the energy-versus-momentum dispersion of the excitations can be inferred, provided the momentum supplied by the lattice can be determined. The present work shows the feasibility of extracting dispersion data from inelastic diffraction measurements. A close analogy is found between inelastic and elastic diffraction (LEED) intensities at normal and at varying incidence, respectively. This identifies the diffracting reciprocal-lattice element and its momentum contribution in the inelastic case. Dispersion data in the 11 azimuth of a tungsten (110) surface are compared with the free-electron volume and surface-plasmon dispersion relations. Discrepancies are found indicating departure from free-electron-like behavior. Also, the excitation which has been previously assigned to a surface plasmon fails to show the appropriate dispersion characteristics. Inner potential corrections are discussed, and the equivalence of the inner potential for elastic and inelastic diffraction is pointed out.

INTRODUCTION

Inelastic electron scattering (IES) is of growing importance in the study of solid surfaces. The full influence of IES in low-energy electron diffraction (LEED) has only recently been recognized. One aspect of the relationship between IES and LEED is combined diffraction and inelastic scattering, i.e., *"inelastic diffraction."*[1-9] Electrons involved in this process are returned to the observer after undergoing a specific energy and momentum loss in the solid. A source of information on electronic excitations, similar to that provided by singly scattered electrons in a characteristic energy loss study, is thus made available.[4] Such information includes dispersion relationships and related excitation probabilities, although this has never been demonstrated in practice. As a result of the variety of possible excitations, the overlapping of scattering cones, and the possibility of reversed sequence in the combined process, the inelastic diffraction pattern may be quite complex. This causes the analysis to be ambiguous with respect to the momentum supplied by the lattice. A possible way of resolving this ambiguity lies in establishing a correlation with LEED data for which the diffracting reciprocal-lattice element can be identified. The main purpose of the present paper is to show the feasibility of extracting excitation dispersion information from inelastic diffraction by correlation with LEED.

Practical reasons for doing inelastic diffraction rather than conventional characteristic loss scattering are as follows. In the former case, the electrons need not penetrate through the sample, and the experiment may be performed at an essentially optional angle of incidence on bulk single crystals. Anisotropy and other properties which depend on bulk crystallography may therefore be studied without the usual limitations imposed by small inelastic scattering angles. Also, the low primary energy provides sensitivity for surface-related effects, as well as for excitations which cannot be observed at the higher energies normally used in characteristic loss measurements.

THEORY

Since inelastic diffraction occurs in a surface region of finite thickness, the total momentum, including the normal component in a limited sense,[10] is conserved. Therefore,

$$\vec{k}_s = \vec{k}_p - \vec{K} + \vec{G} \quad , \tag{1}$$

where $\vec{k}_p$ and $\vec{k}_s$ represent primary (incident) and secondary (emerging) wave vectors, respectively, of the interacting electron. The wave vector $\vec{K}$ of the excitation corresponds to the momentum inelastically lost by the electron, while $\vec{G}$ corresponds to the momentum elastically supplied by the lattice. The primary and secondary electron energies E_p and E_s are related to their respective free-electron momenta by

$$E_p = (\hbar^2/2m)\, k_p^2 \tag{2}$$

and

$$E_s = (\hbar^2/2m)\, k_s^2 \quad . \tag{3}$$

From energy conservation

$$E_p - E_s = E(\vec{K}) \quad . \tag{4}$$

Here, $E(\vec{K})$ expresses the energy-momentum dis-

persion of the excitation. The present goal is to relate $\vec{K}$ to the observable diffraction variables $\vec{k}_p$, $\vec{k}_s$, and thereby determine the form of $E(\vec{K})$.

In order to achieve the required relationship it is first necessary to determine $\vec{G}$, which must at least satisfy the surface Laue condition

$$\vec{G}_{xy} = \vec{G}_{hk} \ , \tag{5}$$

if diffraction is to be observed. Here, $\vec{G}_{xy}$ is the component of $\vec{G}$ in the plane of the surface, while $\vec{G}_{hk}$ is the surface reciprocal-lattice vector (including 2π) which terminates at the hk reciprocal-lattice rod; the pertinent rods lie normal to the surface in the present work. One may relate $\vec{G}$ to the remaining vectors in Eq. (1) through $\vec{k}_i$ and $\vec{k}_d$, which represent the incident and diffracted waves in the diffraction phase of the process, i.e.,

$$\vec{G} = \vec{k}_d - \vec{k}_i \ . \tag{6}$$

Also, since the interaction with the lattice is essentially elastic,

$$k_d = k_i \ . \tag{7}$$

The definitions of $\vec{k}_i$ and $\vec{k}_d$ and conservation of momentum require that

$$\vec{k}_i = \vec{k}_p + a\vec{K} \ , \tag{8a}$$

$$\vec{k}_d = \vec{k}_s + b\vec{K} \ , \tag{8b}$$

where the constants a and b must be determined by experiment. Two possible situations have been discussed in the literature,

$$\left.\begin{aligned} a &= 0 \\ b &= +1 \end{aligned}\right\} \text{ D-IES} \ , \tag{9a, 9b}$$

$$\left.\begin{aligned} a &= -1 \\ b &= 0 \end{aligned}\right\} \text{ IES-D} \ . \tag{10a, 10b}$$

Equation (9) expresses the conditions for diffraction followed by inelastic scattering (D-IES), first proposed by Davisson and Germer to explain an excess inelastic scattering which they found to accompany elastic diffraction.[1] More recent observations of D-IES have been reported.[3,6,8] However, this process is found to be relatively unimportant under the present conditions of observation, which exclude portions of the diffraction pattern occupied by the LEED beams. Equation (10) expresses the conditions for inelastic scattering followed by diffraction (IES-D), which was first proposed by Turnbull and Farnsworth to explain their results.[2] This process has been well confirmed in tungsten by detailed comparisons of elastic and inelastic intensity-versus-energy measurements.[4] Equation (10), rather than Eq. (9), thus applies to the present dispersion analysis.

The momentum relationships applicable to IES-D are summarized schematically in Fig. 1 for diffraction involving the hk reciprocal-lattice rod and in the plane of this rod. In this situation the foregoing equations, with the exception of (4) and (9), lead to the following:

$$\theta_{sc} = \arcsin\left[\sin\theta_s - (E_{hk}/E_s)^{1/2}\right]_{-\theta_p} , \tag{11}$$

$$\theta = \arctan \frac{\sin\theta_s - (E_{hk}/E_s)^{1/2} - (E_p/E_s)^{1/2}\sin\theta_p}{(E_p/E_s)^{1/2}\cos\theta_p - \left\{1 - \left[\sin\theta_s - (E_{hk}/E_s)^{1/2}\right]^2\right\}^{1/2}} \ , \tag{12}$$

$$K = (\hbar/2m)^{-1/2}(E_s)^{1/2}\csc\theta\left[\sin\theta_s - (E_{hk}/E_s)^{1/2} - (E_p/E_s)^{1/2}\sin\theta_p\right] \ , \tag{13}$$

where θ_p and θ_s are the angles of incidence and emergence, respectively, measured relative to the sample normal. Here, θ_{sc} is the inelastic scattering angle, while θ is the angle defining the propagation direction of the excitation. E_{hk} is defined in analogy with Eqs. (2) and (3) by

$$E_{hk} \equiv (\hbar^2/2m)\, G_{hk}^2 \ . \tag{14}$$

Inner potential effects have been neglected in the above considerations. This is justified if the electron is inelastically scattered before entering the crystal, since Eqs. (6) and (7) are valid as long as k_i and k_d *both* represent conditions either inside or outside the crystal. In LEED, this situation corresponds to a lack of dependence of beam positions on inner potential, i.e., there is a compensating refraction when the electron enters and leaves the crystal. In the more general inelastic diffraction situation where inelastic scattering may occur partially, or wholly inside the crystal, the electron energies on entering and leaving may differ, so that the refraction compensation may be incomplete. Consequently, the above derivation is not strictly valid here, and a correction for inner potential must be considered. The expressions replacing Eqs. (11)–(13) when

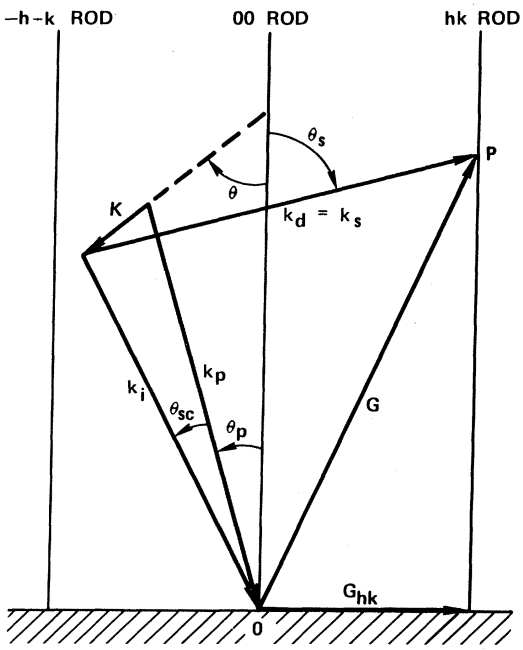

FIG. 1. Wave-vector relationships for IES-D in the *hk* azimuth and involving the *hk* reciprocal-lattice rod. The symbols are defined in the text.

the scattering is entirely within the crystal are derived in the Appendix. These provide a means of placing an upper limit on the correction when the extra kinetic energy E_0 corresponding to the inner potential is given.

Apart from inner potential effects, Eqs. (11)–(13) give conditions for IES-D, provided the dispersion equation [Eq. (4)] is also satisfied for some electronic excitation. If the excitations are appreciably broadened and/or occur with a sufficiently high density in $\vec{K}$ space, Eq. (4) may be partially satisfied by one or more excitations for an arbitrary surface diffraction condition. Some IES-D intensity is then produced whenever $\vec{G}$ terminates on a reciprocal-lattice rod. If, in addition, the termination point (P in Fig. 1) corresponds to a diffraction maximum, e.g., a reciprocal-lattice point, the IES-D intensity is "diffraction enhanced" at the corresponding position in the energy loss spectrum. The diffraction enhancement condition thus corresponds to the condition for a maximum in a LEED intensity-versus-energy curve. If Eq. (4), in addition to Eqs. (11)–(13), is exactly satisfied for one highly probable excitation, the IES-D intensity should show a pronounced maximum. A condition of "excitation enhancement" may then be said to exist. This condition may be superimposed on that of diffraction enhancement, thereby producing doubly enhanced intensity in the loss spectra. The resulting prominent maxima are the experimental basis of the present dispersion analysis. The term "enhanced maxima" will be used to denote the doubly enhanced condition unless the type of enhancement is definitely specified.

EXPERIMENTAL

Briefly, the instrumentation consists of a noncommerical scanning LEED system using a collimating Faraday collector with retarding field energy analyzer. The over-all angular and energy resolutions are roughly 2° and 0.5 eV, respectively. The direct beam measured by the collector is typically in the 10^{-8}-A range, while changes in scattered current in the 10^{-15}-A range are measurable with 0.1-sec response time. Essentially conventional procedures were followed in preparing the tungsten (110) surface. Further details are given in Ref. 4.

The data reduction for the present analysis, including Figs. 3 and 4, was performed manually on retarding curves produced on an X-Y plotter. The reduction consists of locating the energy loss positions of the localized "rises" which correspond to maxima in the energy loss spectra.[4] The point midway between background curves extrapolated from both sides of such a rise was taken as the energy position of the loss maximum, and the corresponding energy loss $E_p - E_s = E$ was referenced to the midpoint of the elastic rise. Recently, a provision for automatic stepping of the retarding potential and digital recording of the collector current at each step was included. This permits data reduction on a Univac 1108, where a convolution operation is applied using fast Fourier-transform programming methods.[11] The operation includes differentiation, optimum smoothing, and unfolding of the directly observed instrumental energy distribution from the recorded data.[12] The elastic component is thereby symmetrized about the zero loss position. This symmetry, combined with the fact that the inelastic spectrum has zero intensity for negative losses, permits subtraction of the elastic component, leaving only the inelastic contribution. Computed roots of the second derivative of the retarding curves give the energy positions of the loss maxima.

RESULTS

Figures 2(a) and 2(b) show a sequence of inelastic electron spectra computed from retarding field data taken at normal incidence and constant collector angle, but at different primary energies E_p on the clean tungsten (110) surface. The collector has been aimed at the position of a strong intensity maximum in the 02 LEED beam which

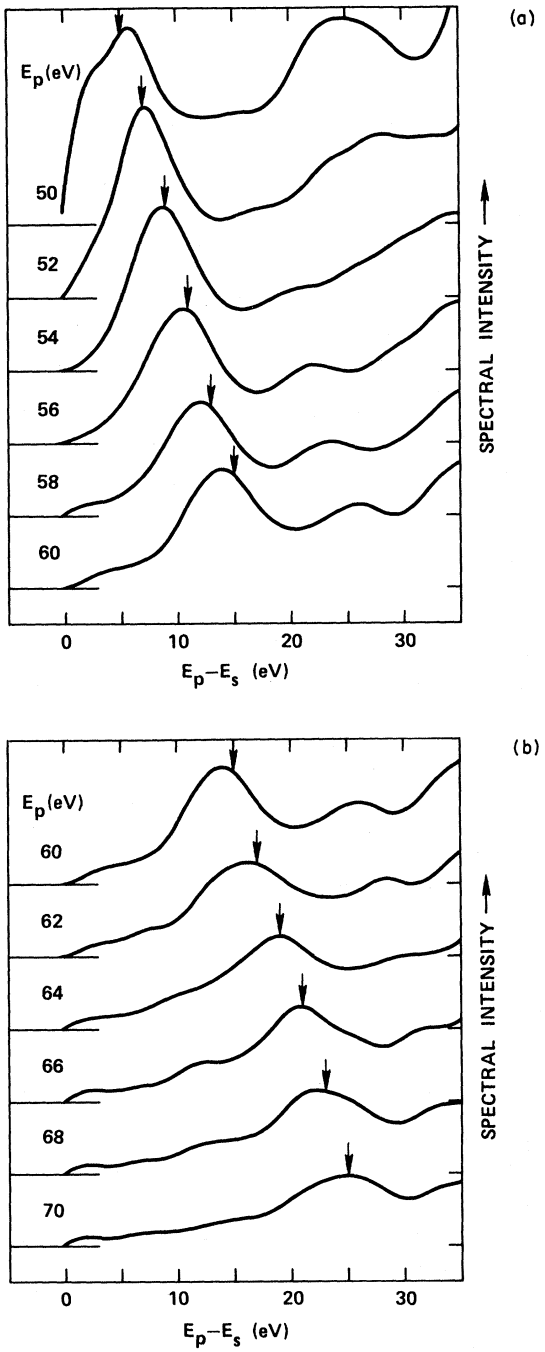

FIG. 2. Sequence of inelastic electron spectra computed from retarding curves measured at normal incidence on the tungsten (110) surface. The collector remains aimed at the position of an intensity maximum in the 02 LEED beam at $E_p \simeq 45$ eV while the primary energy is varied between curves. (a) and (b) cover the ranges $E_p = 50$–60 and 60–70 eV, respectively. The arrows indicate $E_s = 45$ eV, which corresponds to a diffraction enhancement condition for IES-D. Superimposed excitation enhancements occur in the $E_p = 52$-eV and the $E_p = 66$-eV curves.

appears at $E_s = E_p \simeq 45$ eV. Consequently, a condition for IES-D diffraction enhancement is fulfilled near $E_s = 45$ eV, which is indicated by the vertical arrow above each of the spectra. A corresponding maximum is observed in the vicinity of the arrow in each case, in support of the IES-D interpretation. In the $E_p = 52$-eV curve and again, to a lesser extent, in the $E_p = 66$-eV curve, this maximum is relatively large and sharp. Such behavior typifies excitation enhancement. Two examples are thus provided of fully enhanced maxima, i.e., the type used in the dispersion analysis.

By varying both the collector angle and primary energy, the observation of enhanced maxima may be extended to include a variety of excitation and diffraction situations. Figure 3 compares inelastic diffraction at normal incidence with LEED at varying incidence in the 11 azimuth of a tungsten (110) surface. Here, the noncircular symbols indicate positions of observed enhanced maxima as function of the secondary energy E_s and angle θ_s. The loci of the 11 and 22 LEED beams ($E_s = E_p$) at normal incidence are indicated by solid lines. The circles indicate the locations of observed maxima in intensity-versus-energy curves of the 11 LEED beam for angles of incidence in the range $0°$–$10°$. These occupy a limited region above the indicated 11 beam locus, inclusive. Intensity measurements of the 11 and 22 beams below the respective indicated loci in Fig. 3 are beyond the range of the apparatus in its present mode of operation and are therefore excluded. Also, the range $\theta_s < 8°$ is inaccessible at normal incidence.

DISCUSSION

A. Diffraction Analysis

Examination of Fig. 3 shows a predominating coincidence of maxima associated with different energy losses, which implies that the excitation momentum makes no contribution to the diffracted wave vector. This corresponds to $b = 0$ in Eq. (8b), and the fact that $a = -1$ follows immediately from Eqs. (1), (6), and (8). Equation (10) is, therefore, substantiated for most of the maxima shown in Fig. 3. Also, the distribution of inelastic maxima and that of the elastic 11 maxima are essentially the same within the range of present LEED measurements. The analogy of IES-D to LEED, where the varying angle of incidence in the latter case simulates the scattering in the former, is thus verified.

The good agreement between the IES-D and elastic 11 LEED beam maxima in the lower part of the region between the two solid curves indicates that the diffraction here involves the 11 reciprocal-lattice rod. In the range of energies

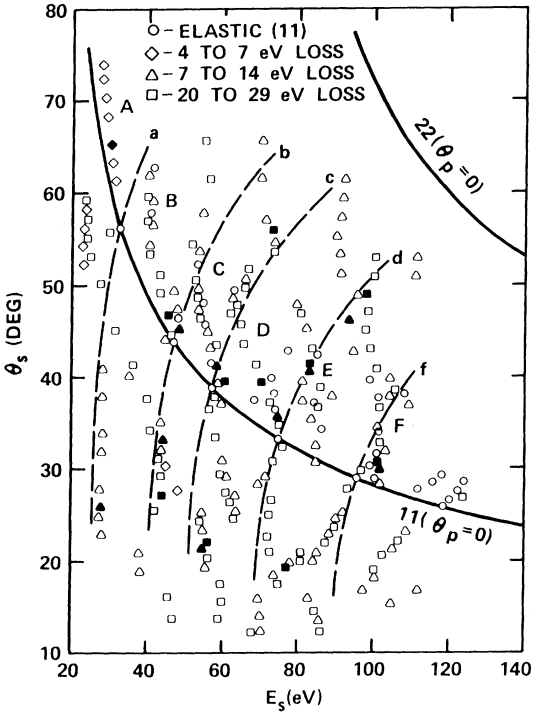

FIG. 3. Angular distribution versus secondary energy of enhanced inelastic diffraction maxima at normal incidence compared to that of 11 LEED maxima at 0°–10° incidence in the 11 azimuth of tungsten (110). Open and solid symbols represent relative and absolute maxima, respectively. The upper and lower solid lines give the positions of the 22 and 11 LEED beams, respectively, at normal incidence. Significance of the dashed lines is explained in the text.

$E_s > 90.0\ \text{eV}/(1+\sin\theta_s)^2$, diffraction by the 22 rod becomes possible, while the 00 rod may, in principle, be involved at any point. However, comparison with intensity in the 00 LEED beam shows agreement with inelastic maxima only in a limited range of θ_s which lies well below the lower solid curve, indicating that IES-D by the 00 rod is improbable above this curve. Because of the large IES-D scattering cone, maxima diffracted by the lattice rods lying in other azimuths may appear in the 11 azimuth. However, azimuthal scans have, as yet, failed to identify any such maxima among those shown in Fig. 3.

Examination of the IES-D maxima assigned to the 11 reciprocal-lattice rod shows that these fall into groups, each of which is designated by a capital letter immediately to the right of the group in Fig. 3. Since the groups coincide with the intensity maxima in the 11 LEED beam, they should also coincide, except for dynamical diffraction effects,[13] with the loci of the 11 Bragg maxima as the angle of incidence is changed. The dashed curves, which are labeled by corresponding lower case letters, indicate the Bragg loci when adjusted to fit the observed LEED maxima at normal incidence by suitably choosing the inner potential.[14] The pronounced departures of the dashed lines from the correspondingly lettered distributions show that the diffraction is dominated by dynamical effects. It is noteworthy, however, that among the enhanced maxima in any given lettered group there are absolute maxima, i.e., maxima of greater intensity than those adjacent, which in several cases lie close to the dashed lines. Corresponding intense maxima in the 11 LEED beam are usually found, indicating a predominantly diffraction origin. However, no consistent LEED counterpart is found for the absolute maxima which, in nearly all of the lettered groups, are found to lie just above the normally incident 11 beam locus in Fig. 3. These possibly result from an excitation probability maximum which lies near the excitation threshold discussed in the next section. If so, similar features should lie just below the indicated beam locus, in a region largely obscured by the proximity of the LEED beam. Some differences in diffraction features associated with IES-D versus LEED may be associated with a difference in penetration depth.[15] A comparative study on tungsten with ordered submonolayer oxygen coverage has shown a systematic difference in the over-all dependence of intensity on energy.[16] The inner potential for IES-D and LEED in clean tungsten is essentially the same, as shown by the agreement in energy positions of the respective maxima in Fig. 3.

B. Excitation Dispersion Analysis

The dispersion analysis is performed on those enhanced maxima which lie above or on the indicated 11 beam locus in Fig. 3. Application of Eqs. (4) and (11)–(14) with $E_{hk} = E_{11} = 22.5$ eV leads to Fig. 4. Here, the excitation energy is plotted versus the relative excitation momentum K/G_{11}, where $G_{11} = 2.43\ \text{Å}^{-1}$. The point coding indicates the angular range of the excitation propagation angle θ for each point. Although correlation with the 11 LEED beam extends only to $\theta_{sc} = 10°$, misidentification of maxima diffracted by the 22 lattice rod is unlikely except for a few points, for which θ and K are both large. The resulting possible ambiguity in Fig. 4 is too slight to influence the present discussion.

The group of points between 20 and 26 eV and the group between 7.5 and 14 eV correspond to excitations previously identified by Tharp and Scheibner[17] as a volume and a surface plasmon, respectively. The upper dashed curve shows the theoretical dispersion of a volume plasmon in a

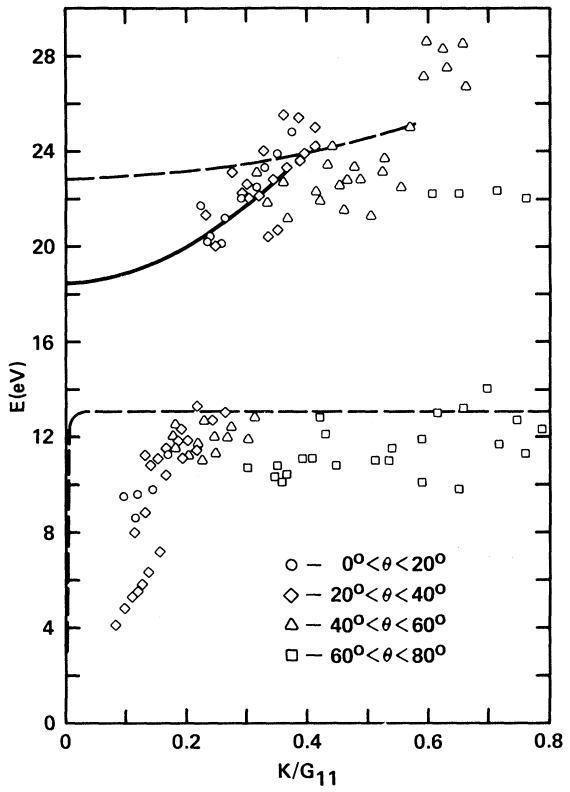

FIG. 4. Excitation dispersion data computed from maxima shown in Fig. 3 on the basis of diffraction by the 11 reciprocal-lattice rod. Different symbols represent the range of the excitation propagation angle for each data point. The significance of the solid and dashed curves is explained in the text.

free-electron gas,[18]

$$E^2(K) = E^2(0) + \tfrac{6}{5}(E_F/m)\hbar^2K^2 \quad , \tag{15}$$

where $E(0) = 22.8$ eV, corresponding to six free electrons per tungsten atom. The Fermi energy E_F is taken as 13.6 eV, which is the average of the two values reported by Mattheiss.[19] The free electron $E(0)$ is found to be in good agreement with the average $E(K)$ observed within the upper group, which confirms Tharp and Scheibner's total scattering measurements.[17] However, the dashed curve provides a poor fit to the present data distribution. The observed dispersion for $K/G_{11} \lesssim 0.5$ is better represented by the solid curve, where $E(0) = 18.5$ eV. The point scatter allows a possible ± 2-eV variation in $E(0)$, which is insufficient to permit good agreement with the free-electron value. Also, m in Eq. (15) must be replaced by an effective mass of $0.5m$ if the above value of the Fermi energy is to be retained. These discrepancies apparently result from failure of the free-electron model for tungsten. The terminations of the upper dashed and solid curves correspond to the theoretical plasmon cutoff wave vectors $K_c = 1.4$ Å^{-1} and $K_c = 0.9$ Å^{-1}, respectively. These values were obtained by solving[18]

$$E(K_c) = (\hbar^2/2m)(2k_FK_c + K_c^2) \quad , \tag{16}$$

where K_F is the wave vector of an electron at the Fermi level, and $E(K_c)$ is given by Eq. (15). The data show some evidence of such a cutoff. However, the relatively few points occurring at $K/G_{11} \gtrsim 0.5$ must be explained. Multiple elastic and quasielastic scattering can change the value of the resultant K without affecting the excitation energy. The excitation energy most likely to be observed in multiple processes is that for which the excitation probability is high, e.g., that corresponding to the absolute maxima lying just above the normally incident 11 beam locus in Fig. 3. For the 20–26-eV group, this energy is about 22 eV, which agrees well with the average energy of the points at large K in this group. The lower K limit of data points represents a threshold for excitation by free electrons in the present energy range. With $E_p \leq 120$ eV, a free electron which loses 20 eV or more energy must lose a minimum momentum equivalent to $K/G_{11} = 0.2$. The threshold momentum is reduced somewhat if internal inelastic scattering with $E_0 > 0$ is included in the model for IES-D. In Fig. 3 the enhanced maximum corresponding to the excitation threshold for given energy conditions always lies on the indicated 11 beam locus, which represents $\theta_{sc} = 0$. Only when the threshold K is very small, or in the case of IES-D involving the 00 rod, does this region of Fig. 3 present experimental difficulties due to the proximity of the LEED beam.

The lower dashed line in Fig. 4 indicates the surface-plasmon dispersion relationship at the boundary of a uniform free-electron material of infinite thickness[18]

$$E^2(K) = (\hbar cK)^2 + [E(0)/\sqrt{2}]^2 - \{(\hbar cK)^4 + [E(0)/\sqrt{2}]^4\}^{1/2} \tag{17}$$

with $E(0) = 18.5$ eV. The dispersion of the 7.5–14-eV group, while of roughly the same general shape, increases much more slowly with increasing K. Also, the wide range of observed θ values is inconsistent with the categorical assignment of this group to a surface plasmon, for which $\theta = \pm 90°$. A partial association with a surface excitation is possible here, however, provided momentum is shared with an excitation which does not propagate along the surface.

The isolated cluster of points around 28 eV apparently represents a separate excitation. Also, the group in the range $E < 7.5$ eV does not join

smoothly with the others, which indicates a separate distinct excitation. The latter group derives exclusively from enhanced maxima found in the A group of Fig. 3, indicating that the excitation probability is high only at primary energies less than 50 eV. This suggests a one-electron, rather than a collective, excitation. The fact that the observed values of θ for the $E_e < 7.5$-eV group are restricted to the range $24°-30°$ probably results from observational limitations imposed by the restriction to low primary energies.

C. Inner Potential Correction

As previously indicated, Eqs. (11)–(13) are based on the assumption that the inner potential is either zero or has negligible influence due to predominantly external inelastic scattering. Figure 4, therefore, rests on the same assumption. Since neither the value of E_0 at low primary energies, nor the situation of the scattering relative to the crystal boundary are well established, an accurate estimate of the resulting error is difficult. However, by estimating E_0 and considering the case of purely internal scattering, where the effect of inner potential is greatest, one may arrive at an approximate upper limit on the error. For purely internal scattering with $E_0 \neq 0$, Eqs. (11)–(13) are replaced by Eqs. (A7)–(A9) of the Appendix, and the fractional correction to K, relative to the case where $E_0 = 0$, is given by Eq. (A10). Figure 5 shows the dependence of this correction on E_0 for three points chosen from Fig. 4, representing each of the four excitations discussed above, except the one for which $E \simeq 28$ eV. The circle on each curve corresponds to $E_0 = 20$ eV, which has been obtained from LEED measurements on a tungsten (110) surface at somewhat higher energies.[13] Thus, the correction may be as large as 10–20%. For larger values of $\sin\theta_s' - (E_{hk}/E_s')^{1/2}$ than those represented in Fig. 5, the correction tends to be smaller, values less than 10% being quite common. Although the effect of the correction is to raise the volume plasmon-energy minimum $E(0)$, this does not amount to more than about 0.5 eV when $E_0 \leq 20$ eV. Also, with this restriction on E_0, the correction is too small to bring the $E < 7.5$-eV group of Fig. 4 into line with the 7.5–14-eV group, thus supporting the identification of the former group with a separate excitation. Some of the scatter in Fig. 4 may be associated with variations in inner potential with electron energy. At low K in particular, where E is rising rapidly with K and single scattering predominates, some systematic discrepancies are found in the E-versus-K dependence of points derived from the different letter groups of Fig. 3. A sufficiently accurate analysis of these discrepancies could provide information on the energy dependence of the inner potential. Another possible source of discrepancy between dispersion points is anisotropy of the dispersion characteristics, although this is difficult to establish from present data in view of the inner potential uncertainty.

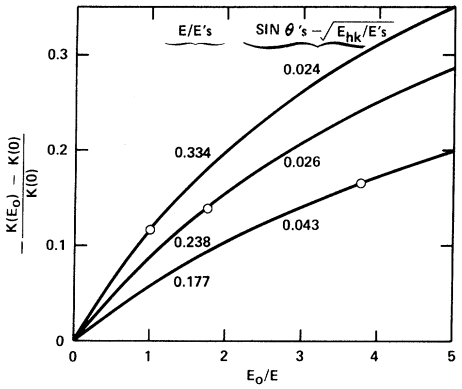

FIG. 5. Variation with relative inner potential of the relative correction for inner potential, assuming internal scattering. Each curve represents a point in a different excitation group in Fig. 4. The corresponding values of E/E_s' and $\sin\theta_s' - (E_{11}/E_s')^{1/2}$, which determine the shape of the curves are given for each curve. The circles indicate the relative correction for $E_0 = 20$ eV. The correction is negative for positive E_0, requiring a shift to lower K values in Fig. 4.

CONCLUSIONS

Inelastic diffraction features arising from IESD at a fixed angle of incidence can be simulated by LEED diffraction features at varying angles of incidence. This provides a means of identifying the diffracting reciprocal-lattice rod in the former case, assuming that the identification can be made in the case of the LEED pattern. As a result, it is possible to determine the momentum vector of an excitation, as well as the energy, and thus to obtain data on its dispersion. Since the exciting electron is not required to pass through the sample, as in the method using high-energy electrons, dispersion measurements can be made on thick bulk single crystals at low energies. In addition to bulk crystallographic effects, a high sensitivity to surface-related effects and to excitations produced only at low primary energy is achieved. Dispersion data on tungsten obtained by the new method show some significant discrepancies with free-electron theory, as might be anticipated. A correction for inner potential may be required if the inelastic scattering occurs predominantly within the surface boundary and if the inner potential is sufficiently large. The ef-

fective inner potential for IES-D is found to be essentially the same as for LEED, in spite of a possible difference in penetration depth for the two processes. Sensitivity of the dispersion data to inner potential provides a possible means of studying the dependence of inner potential on electron energy.

ACKNOWLEDGMENTS

The authors wish to acknowledge the assistance of Robert J. Stirton and Maxine J. Booty, who programmed the computations for the inelastic spectra shown in Fig. 2. They also wish to thank E. Bauer and James L. Stanford for reviewing the manuscript.

APPENDIX

When IES-D occurs within a crystal with inner potential energy $E_0 \neq 0$, one must distinguish between quantities inside (unprimed) and quantities outside (primed) of the crystal. It will be assumed here that the inelastic scattering is entirely internal. Conservation of the tangential component of momentum at the boundary then gives

$$k'_p \sin\theta'_p = k_p \sin\theta_p \ , \tag{A1}$$

$$k'_s \sin\theta'_s = k_s \sin\theta_s \ , \tag{A2}$$

while conservation of energy gives

$$E'_p = E_p - E_0 = (\hbar^2/2m)\, k'^2_p \ , \tag{A3}$$

$$E'_S = E_s - E_0 = (\hbar^2/2m)\, k'^2_s \ . \tag{A4}$$

Equations (1)–(8) and (10), and hence (11)–(14) still apply internally, although Eqs. (2) and (3) can now be justified only on the basis of the free-electron approximation. From Eqs. (2), (A1), and (A3)

$$\theta_p = \arcsin\left(\frac{\sin\theta'_p}{(1+E_0/E'_p)^{1/2}} \right) \ , \tag{A5}$$

while from Eqs. (3), (A2), and (A4),

$$\theta_s = \arcsin\left(\frac{\sin\theta'_s}{(1+E_0/E'_s)^{1/2}} \right) \ . \tag{A6}$$

Equation (11) thus becomes

$$\theta_{sc} = \arcsin\left(\frac{\sin\theta'_s - (E_{hk}/E'_s)^{1/2}}{(1+E_0/E'_s)^{1/2}} \right) - \arcsin\left(\frac{\sin\theta'_p}{(1+E_0/E'_p)^{1/2}} \right) \ . \tag{A7}$$

Equation (12) becomes

$$\theta = \arctan\left(\frac{\sin\theta'_s - (E_{hk}/E'_s)^{1/2} - (E'_p/E'_s)^{1/2} \sin\theta'^2_p}{[(E'_p/E'_s)\cos^2\theta'_p + E_0/E'_s]^{1/2} - \{1 - [\sin\theta'_s - (E_{hk}/E'_s)^{1/2}] + E_0/E'_s\}^{1/2}} \right) \ . \tag{A8}$$

Equation (13) becomes

$$K = (\hbar^2/2m)^{-1/2} (E'_s)^{1/2} \csc\theta [\sin\theta'_s - (E_{hk}/E'_s)^{1/2} - (E'_p/E'_s)^{1/2} \sin\theta'_p] \ , \tag{A9}$$

where θ is given by Eq. (A8). Equation (A9) is of the same form as Eq. (13), so that the inner potential correction enters only through the corrected excitation propagation angle θ. The fractional correction to K may therefore be written

$$[K(E_0) - K(0)]/K(0) = \sin\theta(0)/\sin\theta\,(E_0) - 1 \ , \tag{A10}$$

where $\theta(E_0)$ and $\theta(0)$ are obtained from Eq. (A8) with E_0 set equal to its given value and zero, respectively.

[1] C. Davisson and L. H. Germer, Phys. Rev. 30, 705 (1927).

[2] J. C. Turnbull and H. E. Farnsworth, Phys. Rev. 54, 509 (1938).

[3] P. P. Reichertz and H. E. Farnsworth, Phys. Rev. 75, 1902 (1949).

[4] J. O. Porteus, in *The Structure and Chemistry of Solid Surfaces*, edited by G. Somorjai (Wiley, New York, 1969), p. 12.

[5] W. H. Weber and M. B. Webb, Phys. Rev. 177, 1103 (1969).

[6] M. P. Seah, Surface Sci. 17, 161 (1969).

[7] E. Bauer, Z. Physik 224, 19 (1969).

[8] T. C. Cooper, J. M. Burkstrand, and F. M. Propst, in Proceedings of the Thirtieth Annual Conference on Physical Electronics, Milwaukee, Wisc., 1970 (unpublished).

[9] C. B. Duke and G. E. Laramore, in Proceedings of the Thirtieth Annual Conference on Physical Electronics, Milwaukee, Wisc., 1970 (unpublished); C. B. Duke, G. E. Laramore, and V. Metze (unpublished).

[10] A formal theory of inelastic diffraction phenomena has recently been developed (Ref. 9). An important feature of this theory is nonconservation of the component of momentum normal to the surface. This has a pronounced influence on the predicted shape and broadening of inten-

sity maxima in the energy loss spectrum. However, only the maximal positions which correspond to the most probable momentum exchanges are used in the present analysis; these remain unappreciably affected. In this sense Eq. (1) is valid for the total momentum, including the normal component [C. B. Duke (private communication)].

[11]J. W. Cooley and J. W. Tukey, Math. Comput. 19, 297 (1965).

[12]J. O. Porteus, J. Appl. Phys. 39, 163 (1968).

[13]R. M. Stern and A. Gervais, Surface Sci. 17, 273 (1969).

[14]Actually, the fitting is done by redistributing the reciprocal-lattice points along the 11 rod so as to directly fit the observed 11 LEED maxima at normal incidence. In view of the indexing uncertainty discussed in Ref. 13 and the uncertainty in the value of inner potential at these low energies, no indexing of the redistributed reciprocal-lattice points is attempted. This fitting procedure is essentially equivalent to varying the inner potential to produce direct agreement at normal incidence between each observed LEED maximum and an unspecified Bragg reflection, since the shape of the dashed curves is virtually independent of the assumed value of E_0 over an energy range comparable to the separation of the Bragg reflections.

[15]E. Bauer, J. Vacuum Sci. Technol. 7, 3 (1970).

[16]J. O. Porteus, in Proceedings of the New Mexico Sectional Meeting of the American Vacuum Society, Los Alamos, N. M., 1969 (unpublished).

[17]L. N. Tharp and E. J. Scheibner, J. Appl. Phys. 38, 3320 (1967).

[18]H. Raether, Springer Tracts Mod. Phys. 38, 84 (1965).

[19]L. F. Mattheiss, Phys. Rev. 139, A1893 (1965).

PHYSICAL REVIEW B VOLUME 2, NUMBER 6 15 SEPTEMBER 1970

Diffusion and Correlation Effects in Copper-Zinc Alloys*

N. L. Peterson and S. J. Rothman
Argonne National Laboratory, Argonne, Illinois 60439
(Received 30 January 1970)

The self-diffusion coefficients of copper in copper-zinc alloys containing 0–4-at.% zinc have been measured at 894.4 and 946.7 °C. These results, together with the correlation factor for the diffusion of zinc in copper as determined from measurements of the isotope effect, are used to obtain the relative jump frequencies of the zinc atoms and the neighboring copper atoms by means of the theory of Howard and Manning. The isotope effect for the diffusion of both copper and zinc has been measured in α–Cu-Zn alloys containing 4- and 30-at.% Zn, and in ordered and disordered β–Cu-Zn. The results support Manning's theory of correlation effects in concentrated alloys for those cases where the theory should be applicable (30-at.% Zn and disordered β–Cu-Zn). The agreement is poorer for those cases where the theory is less applicable (4-at.% Zn and ordered β–Cu-Zn). The isotope effect for the diffusion of copper is the same in ordered and in disordered β–Cu-Zn. This supports our earlier conclusion that the Elcock-McCombie mechanism is not the dominant mechanism in ordered β–Cu-Zn when the state of the order is described by $S=0.7$.

INTRODUCTION

The correlation factor f_i for the diffusion of an impurity in an otherwise pure metal can give detailed information on the relative magnitudes of the jump frequencies of the impurity and host atoms. Experimental values of f_i for diffusion in metals can be obtained from measurements of the isotope effect in diffusion[1,2] or from the effect of solute on the self-diffusion of the solvent in dilute alloys.[3] By combining the results of these two types of experiments, the ratios of various atomic jump frequencies about an impurity-vacancy pair can be obtained.[4] Such experiments and calculations were described for the diffusion of zinc in silver in a previous paper[5]; this paper presents similar results for the diffusion of zinc in copper.

Correlation effects in concentrated alloys are more complicated than in dilute alloys; Manning[6] treated them using a rather simplified model. This model is expected to give a more accurate description of correlation effects in concentrated alloys than in dilute alloys, because vacancy binding to the solute becomes more important in the latter. We have attempted to test the range of validity of Manning's theory of correlation effects in binary alloys by measuring the isotope effect for the diffusion of both copper and zinc in copper alloys containing 4- and 30-at.% zinc, and of copper in an alloy containing 50-at.% zinc in both the ordered and disordered states. The results on the alloys containing 50-at.% zinc together with our previous results on the isotope effect for the diffusion of zinc in the same alloy[7] allow us to draw qualitative conclusions about the mechanism of diffusion in β–Cu-Zn.